Chapter 4

Spectroscopic features of Ni^{2+} ions in tellurite-arsenate glass system

$20ZnF_2$–$30As_2O_3$–$(50-x)TeO_2$: xNiO ($0 \leq x \leq 2.0$) glasses were synthesized. The glasses were characterized by X-ray diffraction, scanning electron microscopy, EDS and DSC techniques. A variety of properties, i.e. optical absorption, infrared, magnetic susceptibilities and dielectric properties (constant ε', loss tan δ, ac conductivity σ_{ac} over a wide range of frequency and temperature) of these glasses have been carried out. The analysis of results of all these studies has indicated that the nickel ions occupy both octahedral and tetrahedral positions and the gradual increase of NiO content in the glass matrix causes a growing proportions of Ni^{2+} ions that occupy octahedral positions. The luminescence spectra of these glasses have exhibited a broad emission band in region 1200–1450 nm identified due to $^3T_2(3F) \rightarrow {}^3A_2(3F)$ octahedral transition of Ni^{2+} ions. The luminescence efficiency and cross section have been found to be the highest for the glass containing highest concentration of NiO. Finally it is concluded that higher the concentration of octahedrally positioned Ni^{2+} ions, higher is the luminescence efficiency and such glasses may be useful for broad band optical amplifiers in NIR region.

Spectroscopic features of Ni^{2+} ions in tellurite-arsenate glass system

4.1. Introduction

Now–a–days, intense investigations are being carried out for the development of the materials suitable for ultra broad band optical amplifiers to revolutionize the telecommunication systems. Though, the rare earth ions doped glasses were considered as the suitable candidates for such applications, the optical amplification band width in these materials is very low since the emission bands of 4f–4f transition of the rare earth ions are very narrow. In view of this, large number of investigations are being carried out for exploring possibility of lasing emission by the transition metal oxides of Ti, Cr, Mn, V, Ni, Mo etc. in various glass matrices [1–5]. Among these, Cr^{4+} ions containing glasses have been used as potential candidates for high gain optical amplifiers with larger bandwidths in glass materials; nevertheless, the chromium ions exist in multi valent states, viz., Cr^{3+}, Cr^{4+}, Cr^{5+} and Cr^{6+} . The same is true in case of other transition metal ions like Ti, Mn, V. Hence, it is too difficult to have the strict control over the required or suitable valence state of these ions in the glass matrix to get the luminescence. Unlike these ions, the nickel ions mostly exist in divalent state and are extremely stable and there is no need of any special care in experimentation in retaining nickel ions in divalent state. Ni^{2+} ions exhibit several strong absorption bands in the visible and NIR regions

where the pumping sources are easily available. The octahedrally positioned Ni^{2+} ions in glass network are expected to exhibit eye safe laser emission of wavelength at about 1.5 μm due to $^3T_2 \rightarrow {}^3A_2$ transition even at room temperature, this transition is of great importance in telecommunications [6]. There have been considerable recent studies on lasing action of nickel ions in various glass and glass ceramic materials [7, 8]. As described above tellurium arsenate glass network offers a highly suitable environment for hosting the lasing nickel ions. Thus this chapter is devoted mainly to throw some light on the emission characteristics of nickel ions in the IR region in ZnF_2–As_2O_3–TeO_2 glass system. The studies undertaken are, optical absorption, IR and photoluminescence after the characterization of the glasses by X–ray diffraction, energy dispersive spectroscopy and thermal analysis. The magnetic and dielectric studies are also taken up to have some additional information on the environment of the nickel ions in the glass matrix.

4.2 Brief review of the studies on glasses containing nickel ion

In this review a brief report on the glasses containing nickel ion including some tellurite glasses has been presented.

Souri and Salehizadeh [9] have investigated the effect of NiO content on the optical band gap, refractive index, and density of TeO_2-V_2O_5-NiO glasses. These results have indicated that the values of optical band gap decrease from 2.02 to 1.64 eV and the static refractive index increase from 1.309 to 1.673 as

the NiO content increases in the glass matrix. Moustaffa *et al.* [10] have investigated ultraviolet and visible absorption of some sodium and potassium silicate glasses containing nickel oxide, ferric oxide or both nickel and ferric oxides. These studies have revealed no ultraviolet absorption bands but showed characteristic visible absorption bands due to octahedral and tetrahedral coordinations. The analysis of these results has indicated that the proportion of tetrahedral units increases with the increase in the alkali oxide content. Kumar *et al.* [11] have studied the effect of NiO on the phase formation, thermo-physical properties and sealing behaviour of lithium zinc silicate glass-ceramics. This study has indicated that the addition of NiO favoured inter-diffusion of species at the interface leading to better sealing. Prasad *et al.* [12] have investigated the influence of nickel ions on dielectric and other physical properties of PbO-MoO_3-B_2O_3 glass system. In this study it was reported that there is an increase in the rigidity and the dielectric breakdown strength of this glass system when the concentration of NiO is around 0.6 mol %. Bao *et al.* [13] have reported luminescence properties of nickel and bismuth co-doped barium aluminosilicate glasses. In this study the authors have observed visible luminescence at about 425 nm and broadband infrared luminescence at about 1330 nm when excited by ultraviolet light and 808 nm laser diode, respectively. The intensity of the two emission bands were found to decrease with increasing NiO concentration. The mechanisms of the observed

phenomena were discussed in detail. Kusatsugu *et al.* [14] have synthesized oxyfluoride glass ceramics with a small amount of NiO by spatially selected crystallization by irradiations of continuous wave lasers with a wavelength of λ=1064 or 1080 nm. From this study it was concluded that a combination of Ni^{2+} dopings and laser irradiations is effective in spatially selected local crystallizations of fluorides in oxyfluoride glasses.

Wang and Liang [15] have reported crystallization behavior and infrared radiation property of nickel-magnesium cordierite based glass-ceramics by means of differential thermal analysis, X-ray diffraction and scanning electron microscopy. The infrared radiation property of this material was examined via the measurement of the whole-band normal direction emissivity. The results demonstrated that the adding of NiO can suppress the precipitation of μ-cordierite and promote the crystallization of α-cordierite in $MgO\text{-}Al_2O_3\text{-}SiO_2$ glasses. Sato *et al.* [16] have prepared some NiO-doped Bi_2O_3,La_2O_3-SrO-$BaO\text{-}Nb_2O_5\text{-}B_2O_3$ glasses and SBN crystal lines have been patterned on the glass surface by heat-assisted laser irradiation and scanning of continuous-wave Nd:YAG laser. This study demonstrated that a combination of Nd:YAG laser and Ni^{2+} ions is a novel technique for spatially selected crystallization of SBN crystals in the glass. Wu *et al.* [17] have reported broadband infrared luminescence centered at 1310 nm with full width at half maximum of about 300 nm in Ni^{2+}- doped $ZnO\text{-}Al_2O_3\text{-}SiO_2$ system glass-ceramics. The peak

position of the infrared luminescence showed a blue-shift with increasing heat-treatment temperature, but a red-shift with an increase in NiO concentration. The mechanisms of the observed phenomena were discussed and concluded that these glass-ceramics are promising as materials for super broadband optical amplifier and tunable laser. Mejia-Ramirez *et al.* [18] have investigated the structural behavior of nickel oxide in Na_2O-CaO-MgO-Fe_2O_3-Al_2O_3-SiO_2 glassy and glass-ceramic materials. In this study it was shown that NiO promoted the formation of bunsenite crystals, as nuclei for crystallization. It was also reported that NiO promoted formation of pyroxenes even for compositions with low MgO contents, which formed gehlenite without NiO admixtures. Suzuki *et al.* [19] have investigated the crystallization processes of Li_2O-Ga_2O_3-SiO_2-NiO glass system. In this study it was reported that transparent glass-ceramic containing $LiGa_5O_8$:Ni^{2+} as the sole crystalline phase was obtained from glass with the composition of $13Li_2O$-$23Ga_2O_3$-$64SiO_2$-0.1NiO (in mol%) by the heat treatment in the temperature range from 923 to 953 K. Optical absorption measurements on these glasses have revealed that doped Ni^{2+} occupied five-folded trigonal bipyramidal sites in the as-quenched glass matrices but six-folded octahedral sites of precipitated $LiGa_5O_8$ in the glass-ceramics. These authors have also reported [20] broadband near-infrared emission in the wavelength region from 1100 nm to 1600 nm, attributed to $^3T_{2g} \rightarrow {}^3A_{2g}$ transition of octahedral Ni^{2+}. The emission lifetime was measured at

more than 900 μsec at 5 K and 500 μsec even at 300 K. The emission quantum efficiency was measured by using an integration sphere. It was about 9.1 %, which is enough high as a practical gain medium.

Brendeback *et al.* [21] investigated the effect of NiO dopant concentration in sodium metaphosphate glasses by means of X-ray absorption fine structure and UV/VIS/NIR spectroscopic investigations. Schlenz *et al.* [22] have carried out high energy X-ray diffraction studies on Ni doped sodium metaphosphate glasses. From these studies they have evaluated the average Ni-O distance as 2.03 A^o and the coordination of the nickel ion as in the glass network as 6.0. Rao *et al.* [23] reported the optical absorption and thermoluminescence properties of antimony borate glasses doped with NiO. The results were analyzed in the light of different environments of nickel ions. Tawati and Adlan [24] have recently reported thermoelectric power of semiconducting cobalt phosphate glasses mixed with nickel oxide. These investigations have provided the information on the polaron formation and the disorder energy due to random fields in the glass matrix. Kundu and Chakravorty [25] have investigated nickel the structural properties of titania glasses and concluded that the glass structure is built up by cross linking of NiO_3 triangular units with TiO_6 octahedron. Singh and Singh [26] reported thermodynamic activity of nickel oxide in alkali silicate glasses and found that the activity coefficient of nickel oxide decreases with temperature. El-Desoky

et al. [27] have studied magnetic and electrical properties of lithium borosilicate glasses containing nickel oxide. Rajendran *et al.* [28] have reported the propagation of ultrasonic waves in nickel doped calcium aluminoborate glasses. Shibata *et al.* [29] have reported studies of NiO dissolved alkali silicate glasses based on redox potential and visible absorption spectra. From the studies they have concluded that the Ni^{2+} ions exist in tetrahedral and octahedral coordinations in these glasses. The studies also revealed that the relative ratio of tetrahedral to octahedral species of Ni^{2+} depends on the concentration of NiO. Musinu and Piccaluga [30] have investigated the environment of nickel ions in alkali phosphate glasses by X-ray diffraction and determined the coordination of nickel ions.

Corrias *et al.* [31] have studied the structure of nickel phosphate glasses by neutron scattering with isotropic substitution for nickel. Kashif *et al.* [32] have studied the structure and magnetic susceptibility of sodium borate glasses containing nickel oxide. Khalifa *et al.* [33] have investigated the effect of duration of melting on the absorption spectra, molar volume and refractive index of nickel containing glasses. Rao *et al.* [34] have studied optical absorption spectra of Ni^{2+} ions in lead acetate glasses and interpreted the absorption bands in terms of ligand field theory. Baiocchi *et al.* [35] have studied optical and magnetic properties of nickel ions in lead silicate glasses; they have found that Ni^{2+} ions are both four fold and six fold coordinated in the glasses. They have

assigned the bands observed in the optical absorption spectrum to the corresponding transitions on the basis of ligand field calculations. Paul and Tiwari [36] from their studies on Ni^{2+} ions in silicate glasses have concluded that Ni^{2+} can behave as network formers in the right conditions of temperature and composition.

In spite of this literature, still there is a lot of scope to investigate the influence of nickel ions on physical properties of ZnF_2–As_2O_3–TeO_2 glass system.

4.3 Results

For the present study, a particular composition $20ZnF_2$–$30As_2O_3$–$(50\text{-}x)TeO_2$: xNiO (with x ranging from 0 to 2.0) is chosen. The details of the composition are:

N_0:$20ZnF_2$–$30As_2O_3$–$50TeO_2$

N_2:$20ZnF_2$–$30As_2O_3$–$49.8TeO_2$:0.2NiO

N_4:$20ZnF_2$–$30As_2O_3$–$49.6TeO_2$:0.4NiO

N_6:$20ZnF_2$–$30As_2O_3$–$49.4TeO_2$:0.6NiO

N_8:$20ZnF_2$–$30As_2O_3$–$49.2TeO_2$:0.8NiO

N_{10}:$20ZnF_2$–$30As_2O_3$–$49.0TeO_2$:1.0NiO

N_{15}:$20ZnF_2$–$30As_2O_3$–$48.5TeO_2$:1.5NiO

N_{20}:$20ZnF_2$–$30As_2O_3$–$48.0TeO_2$:2.0NiO

The physical parameters such as nickel ion concentration N_i, mean nickel ion separation r_i, molar volume (V_M) of these glasses are evaluated from the measured values of density d and calculated average molecular weight $\overline{M}$ using the conventional formulae and are presented in Table 4.1.

Table 4.1 Physical parameters of ZnF_2–As_2O_3–TeO_2:NiO glasses.

Glass	Conc. NiO (mol%)	Avg. Mol. Wt. $\overline{M}$	Density (g/cm^3)	Molar volume V_m (cm^3/mole)	Total nickel ion conc. N_i (10^{19}/cm^3)	Inter ionic distance of nickel ions r_i (A^o)	Polaron radius r_p (A^o)
N_0	0	159.83	5.3038	30.13	-	-	-
N_2	0.2	159.66	5.3057	30.09	4.00	29.23	11.78
N_4	0.4	159.49	5.3108	30.03	8.02	23.19	9.34
N_6	0.6	159.32	5.3138	29.98	12.1	20.24	8.16
N_8	0.8	159.15	5.3189	29.92	16.1	18.38	7.41
N_{10}	1.0	158.98	5.3277	29.84	20.2	17.05	6.87
N_{15}	1.5	158.55	5.3432	29.67	30.4	14.86	5.99
N_{20}	2.0	158.13	5.3529	29.54	40.8	13.49	5.43

The X–ray diffraction pattern (Fig. 4.1) of ZnF_2–As_2O_3–TeO_2: NiO samples indicated virtually no crystallinity. The chemical makeup of the glasses is evaluated using EDS (Fig. 4.2); the EDS analysis indicates the presence of Te, Zn, O, F, As and Ni elements in the glass samples.

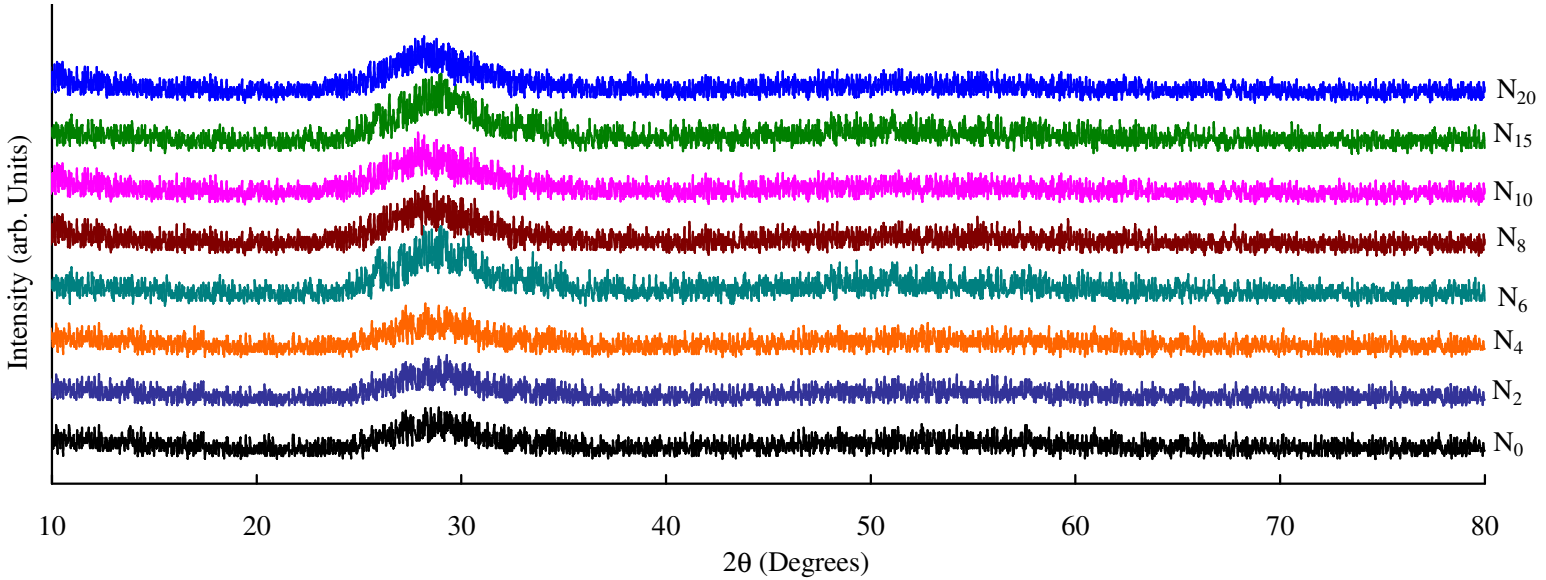

Fig. 4.1 X-Ray Diffraction pattern of ZnF_2–As_2O_3–TeO_2: NiO glasses.

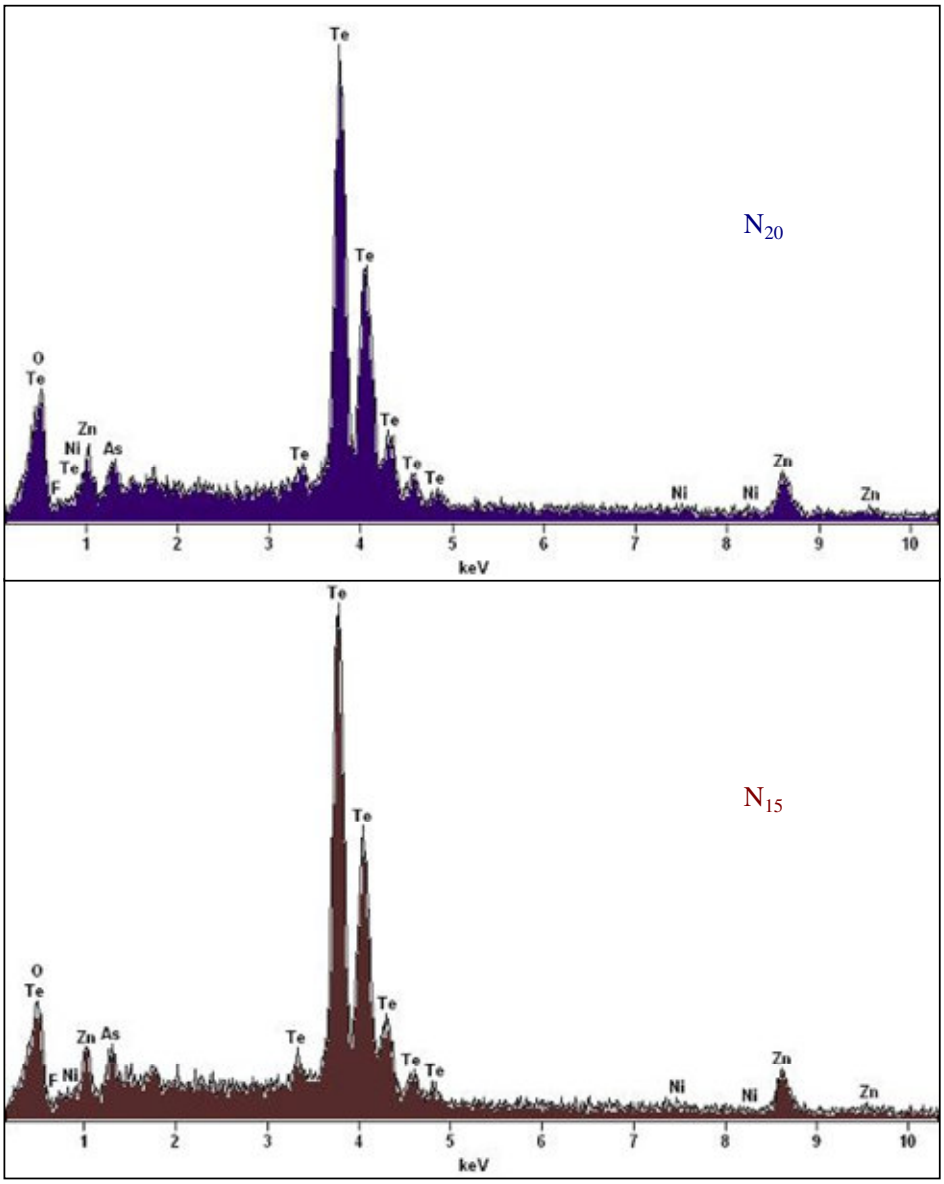

Fig. 4.2 EDS of ZnF_2–As_2O_3–TeO_2: NiO glasses.

Fig. 4.3 represents differential scanning calorimetric (DSC) scan of ZnF_2–As_2O_3–TeO_2 glass doped with 0.4 mol% NiO. The trace has exhibited an endothermic effect due to glass transition at about 290 ^oC followed by a well–defined exothermic effect due to crystallization temperature (T_C). The trace also exhibited another endothermic effect due to melting temperature at 580 ^oC. The DSC scans for other glasses have exhibited the similar behaviour. The variation of glass transition temperature (T_g), (T_C–T_g), (T_m–T_C) and glass forming ability parameter (K_{gl}) with concentration of NiO are shown as insets of Fig. 4.3. These parameters have been observed to decrease with the concentration of NiO (Table 4.2). To observe the mass change effects during heating process, we have also recorded thermal gravimetric traces for all the samples; in Fig. 4.3, TG trace for one of the glasses (N_4) is shown. The trace predicts that decomposition process involves three successive steps. First, decreasing mass of samples (mass reduction temperature onset), second increasing of mass up to mass increase temperature peak and rapid mass lowering to residual mass; the mass increasing peak is well corresponding with crystallization peak. The TGA traces for other glasses found to exhibit similar behaviour.

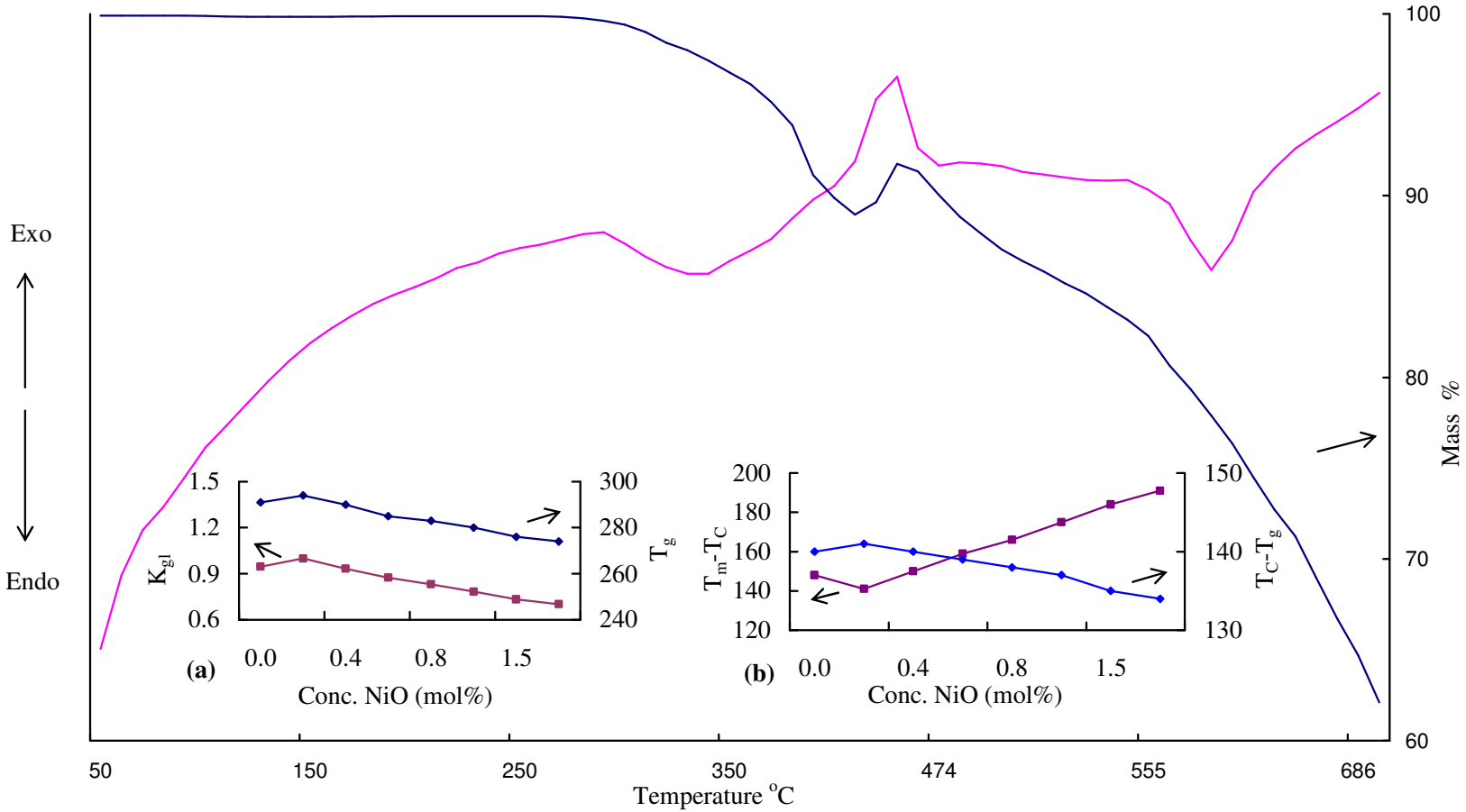

Fig. 4.3 DSC trace and weight loss of ZnF_2–As_2O_3–TeO_2 glass doped with 0.4 mol% of NiO. Inset (a) shows the variation of T_g and K_{gl} and (b) represents the variation of (T_C–T_g) and (T_m–T_C) with the concentration of NiO.

Table 4.2 DSC data of ZnF_2–As_2O_3–TeO_2:NiO glasses.

Glass	T_g (^oC)	T_c (^oC)	T_m (^oC)	T_c-T_g (^oC)	K_{gl} = $(T_C-T_g)/(T_m-T_C)$
N_0	291	431	579	140	0.946
N_2	294	435	576	141	1.000
N_4	290	430	580	140	0.933
N_6	285	424	583	139	0.874
N_8	283	421	587	138	0.831
N_{10}	280	417	592	137	0.783
N_{15}	276	411	595	135	0.734
N_{20}	274	408	599	134	0.702

Fig. 4.4 represents the optical absorption spectra of ZnF_2–As_2O_3–TeO_2:NiO glasses recorded at room temperature in the wavelength region 400–1500 nm. The absorption edge observed at 414 nm for glass N_2 is observed to shift towards slightly higher wavelength side with increase in the concentration of NiO. From the observed absorption edges, the optical band gaps (E_0) of these glasses are evaluated by drawing Urbach plots (Fig. 4.5) between $(\alpha\hbar\omega)^{1/2}$ and $\hbar\omega$. The value of the optical band gap is observed to be the highest for the glass N_2. Additionally, the spectrum of the sample (N_2) exhibited, three clearly resolved intense absorption bands in the NIR and visible regions at 1310 nm (O_{h1}), 795 nm (O_{h2}) and 718 nm (T_{d2}). As the concentration of NiO is increased, the intensity of the octahedral bands (O_h bands) is observed to increase with a shift towards slightly higher wavelength;

the intensity of the tetrahedral band is observed to decrease with a slight shift in the band position towards lower wavelength. The summary of the data on the positions of various absorption bands is furnished in Table 4.3 along with the other pertinent data on optical absorption spectra of these glasses.

Table 4.3 Data on optical absorption spectra of ZnF_2–As_2O_3–TeO_2:NiO glasses

Band position (nm) ↓ Glass →	N_2	N_4	N_6	N_8	N_{10}	N_{15}	N_{20}
$^3T_1(F)\rightarrow{}^3T_1(P)$	718	717	714	710	708	706	704
$^3A_2(F)\rightarrow{}^3T_1(F)$	795	796	797	798	799	801	802
$^3A_2(F)\rightarrow{}^3T_2(F)$	1310	1313	1315	1316	1317	1318	1320
Cut-off wavelength (nm)	414	432	436	440	447	452	459
Optical band gap E_o (eV)	2.84	2.74	2.69	2.62	2.58	2.54	2.49
Dq (cm^{-1})	762.4	761.1	760.0	759.2	758.5	757.2	756.2
B (cm^{-1})	778.9	777.5	776.4	775.6	774.8	773.6	772.5
C (cm^{-1})	3271	3265	3261	3258	3254	3249	3245
Nephelauxetic ratio (β)	0.756	0.755	0.754	0.753	0.752	0.751	0.750

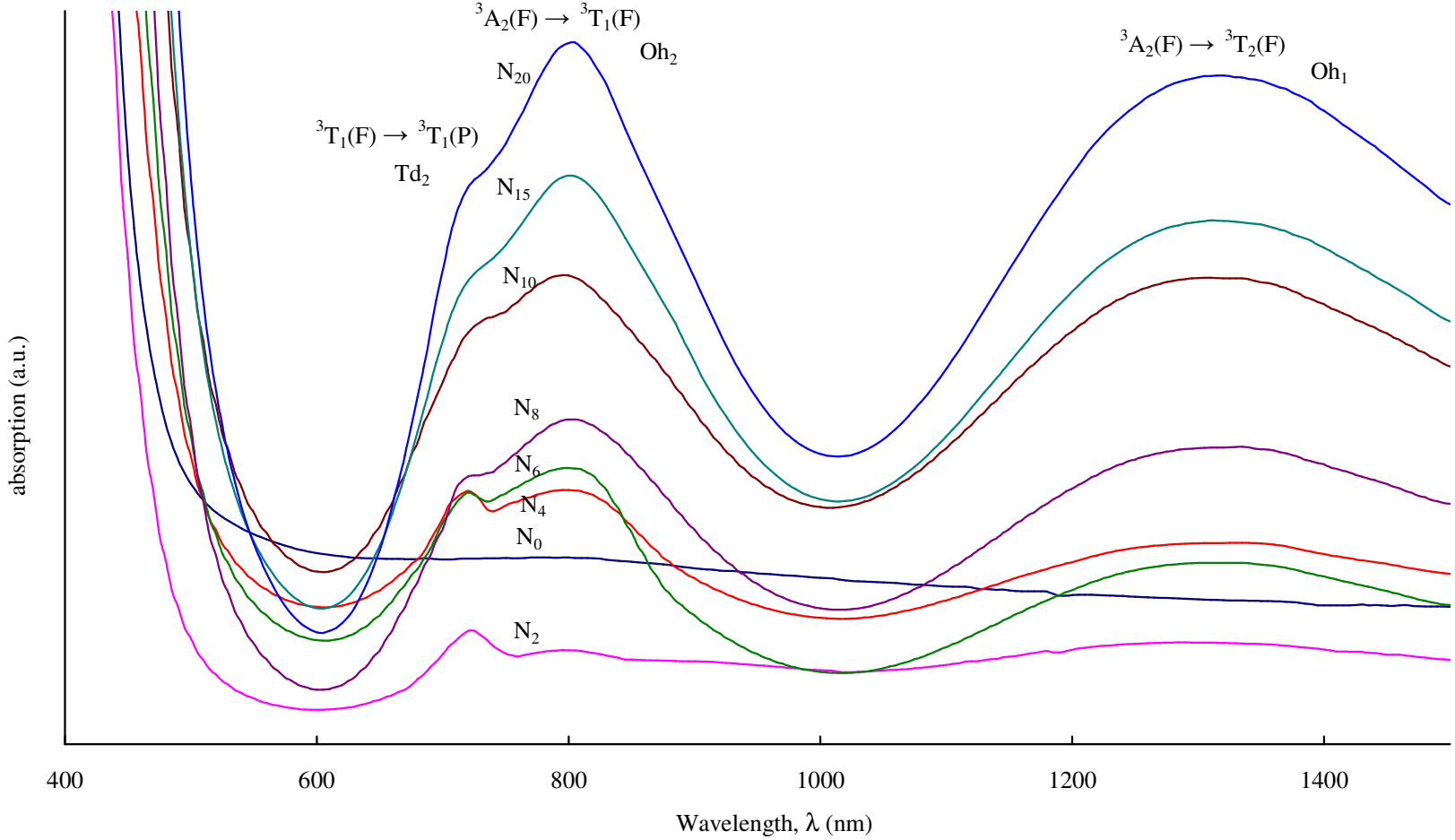

Fig. 4.4 Optical absorption spectra of ZnF_2–As_2O_3–TeO_2:NiO glasses.

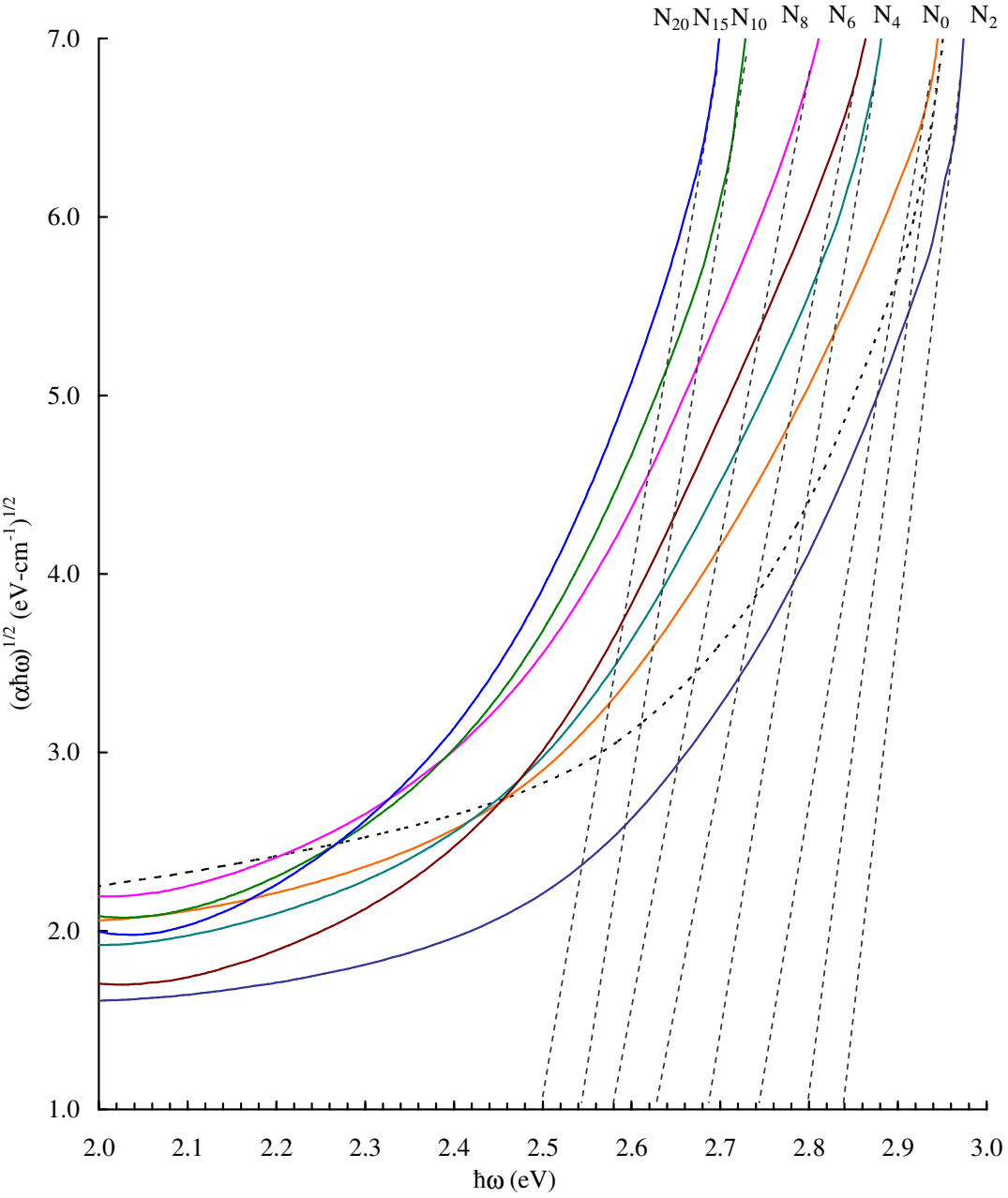

Fig. 4.5 Urbach plots to evaluate optical band gaps for ZnF_2–As_2O_3–TeO_2:NiOglasses.

Fig. 4.6 shows the photoluminescence spectra of ZnF_2–As_2O_3–TeO_2: NiO glasses recorded at room temperature with the excitation wavelength of 800 nm. The spectrum of each glass exhibited a broad emission band in the region 1200–1450 nm; this band is identified due to $^3T_2(3F) \rightarrow {}^3A_2(3F)$ transition of nickel ion. With the increasing content of nickel ions in the glass matrix, the half width of the band is observed to increase with a shift of the peak position towards slightly higher wavelength (Table 4.4).

Table 4.4 Summary of data on photoluminescence of ZnF_2–As_2O_3–TeO_2:NiO glasses

Sample	Emission peak position (nm)	Refractive index	σ_p^E (10^{33}, cm^2)
N_2	1330	1.651	1.113
N_4	1333	1.659	1.126
N_6	1337	1.664	1.135
N_8	1340	1.668	1.143
N_{10}	1344	1.673	1.146
N_{15}	1349	1.678	1.148
N_{20}	1354	1.683	1.151

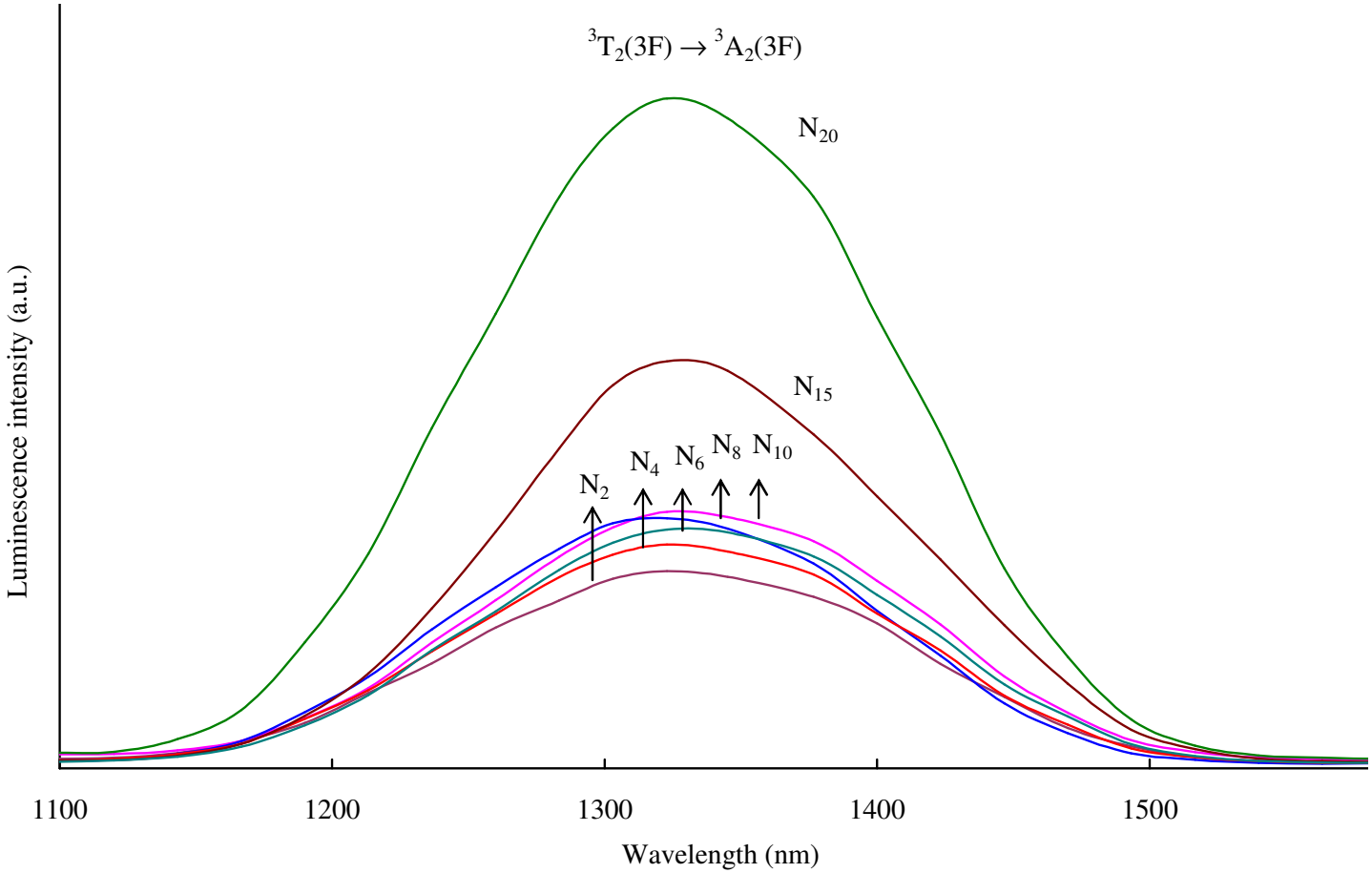

Fig. 4.6 Photoluminescence spectra of ZnF_2–As_2O_3–TeO_2:NiO glasses recorded at room temperature (λ_{exc}= 800 nm).

Fig. 4.7 shows infrared transmission spectra of ZnF_2–As_2O_3–TeO_2: NiO glasses. The spectra exhibited different absorption bands due to various structural units of TeO_2 and As_2O_3. IR spectrum of crystalline TeO_2 is expected to exhibit two absorption bands at 772 cm^{-1} [$\nu_1(A_1)$] and at 650 cm^{-1} [$\nu_2(A_2)$] due to ν_s–TeO_{2eq} and ν_s–TeO_{2ax} vibrations with C_{2v} symmetry, respectively [37]. Similarly four prominent bands are expected in the IR spectrum of crystalline As_2O_3 due to ν_1 (1050 cm^{-1}), ν_2 (625 cm^{-1}), ν_3 (812 cm^{-1}) and ν_4 (495 cm^{-1}) vibrations of AsO_3 structural units [38]. In the spectrum of glass N_0 the axial band due to vibrations of ν_s–TeO_{2ax}, is located at 643 cm^{-1} whereas the ν_s–TeO_{2eq} band is observed to be missing; the ν_1 and ν_2–bands of AsO_3 structural groups are located at 1007 and 620 cm^{-1} respectively; the ν_4-band of these structural groups is also positioned at about 431 cm^{-1}. With the introduction of NiO, the ν_s–TeO_{2ax} and ν_2 of AsO_3 bands are shifted gradually towards higher frequencies with a considerable decrease in the intensity. The summary of various band positions of the IR spectra of these glasses is furnished in Table 4.5.

Table 4.5 IR spectral band positions (in cm^{-1}) of ZnF_2–As_2O_3–TeO_2:NiO glasses.

Assignment	Glass N_0	Glass N_2	Glass N_4	Glass N_6	Glass N_8	Glass N_{10}	Glass N_{15}	Glass N_{20}
ν_1 - As_2O_3	1007	1012	1019	1037	1054	1069	1077	1091
ν^s_{ax} - TeO_2	643	646	650	651	653	655	657	658
ν_2 - As_2O_3	620	621	625	628	631	632	634	636
ν_4 - As_2O_3	431	434	435	438	440	441	444	447

Magnetic susceptibility of ZnF_2–As_2O_3–TeO_2 glasses measured at room temperature is observed to increase with NiO content in the glass composition (Table 4.6). From the values of magnetic susceptibilities, effective magnetic moments of nickel ions in the glasses are evaluated and presented in Table 4.6. The value of μ_{eff} is found to be in the range of 4.0–3.7μ_B for glasses N_2–N_6 and for the glasses N_8–N_{20}, it is found to be in the range of 3.45–3.0μ_B.

Table 4.6 Summary of the data on magnetic properties of ZnF_2–As_2O_3–TeO_2:NiO glasses.

Glass	Conc. NiO (mol%)	Magnetic susceptibility χ (x10^{-6} emu)	Magnetic moment μ_{eff} (μ_B)
N_2	0.2	4.36	4.00
N_4	0.4	7.89	3.80
N_6	0.6	11.24	3.70
N_8	0.8	13.05	3.45
N_{10}	1.0	15.89	3.40
N_{15}	1.5	23.69	3.38
N_{20}	2.0	24.99	3.00

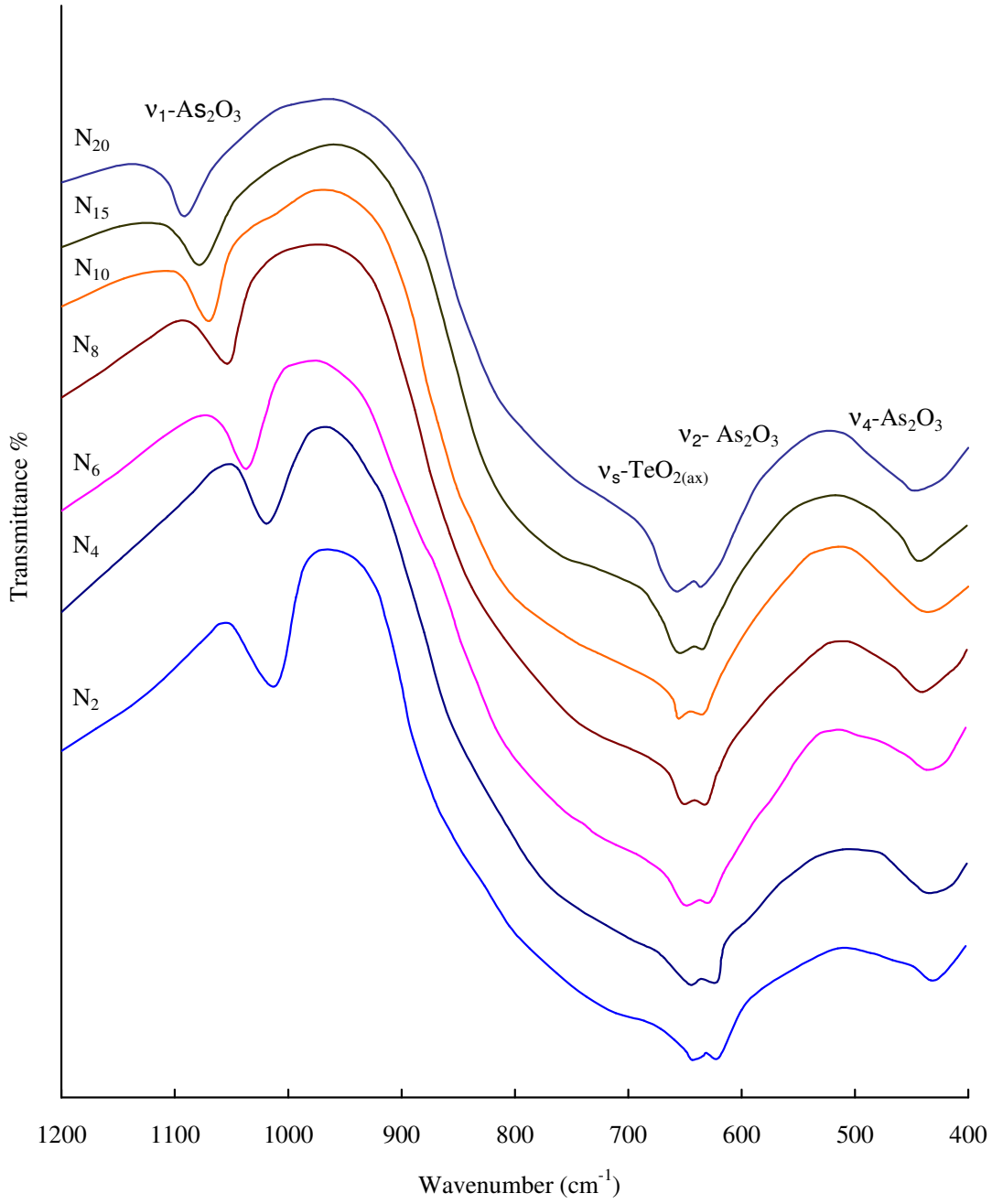

Fig. 4.7 IR spectra of ZnF_2–As_2O_3–TeO_2:NiO glasses.

The dielectric constant ε' and loss tan δ at room temperature (≈ 30 ^{o}C) of nickel free ZnF_2–As_2O_3–TeO_2 glasses at 100 kHz are measured to be 18.5 and 0.008 respectively. Fig. 4.8 represents the variation of dielectric constant (ε') and loss (tan δ) with temperature at different frequencies of ZnF_2–As_2O_3–TeO_2 glasses doped with 2.0 mol% of NiO. The temperature dependence of ε' at 1 kHz of ZnF_2–As_2O_3–TeO_2 glasses doped with different concentrations of NiO is shown in Fig. 4.9(a). The value of $\varepsilon^{'}$ is found to exhibit a considerable increase at higher temperatures especially at lower frequencies; the rate of increase of $\varepsilon^{'}$ with temperature is found to increase with increase in the concentration of dopant.

A comparison plot of variation of tan δ with temperature, measured at a frequency of 10 kHz for all glasses is presented in Fig. 4.9(b). The loss curves have exhibited distinct maxima; with increase in frequency the temperature maximum of tanδ shifts towards higher temperatures and with increase in temperature, the frequency maximum shifts towards higher frequencies, indicating the relaxation character of dielectric losses in these glasses. From these curves, it is also observed that the region of relaxation shifts towards lower temperatures with broadening of relaxation peak and increasing value of $(\tan \delta)_{max}$ with increase in the concentration of the NiO. The effective

activation energy W_d for the dipoles is evaluated for all the glass samples using the relation

$$f = f_o e^{-W_d / kT} \tag{4.1}$$

and its variation with the concentration of NiO is shown as the inset of Fig. 4.9; the activation energy is found to decrease gradually with increase in the concentration of the NiO. The ac conductivity σ_{ac} is calculated at different temperatures, using (eq. 3.1) for different frequencies and the plots of log σ_{ac} against 1/T are shown in Fig. 4.10 for all the glasses at 100 kHz. From these plots, the activation energy for conduction in the high temperature region over which a near linear dependence of log σ_{ac} with 1/T could be observed is evaluated and its variation with the concentration of NiO is shown as the inset of Fig. 4.10; this activation energy is also found to decrease gradually with increase in the concentration of NiO.

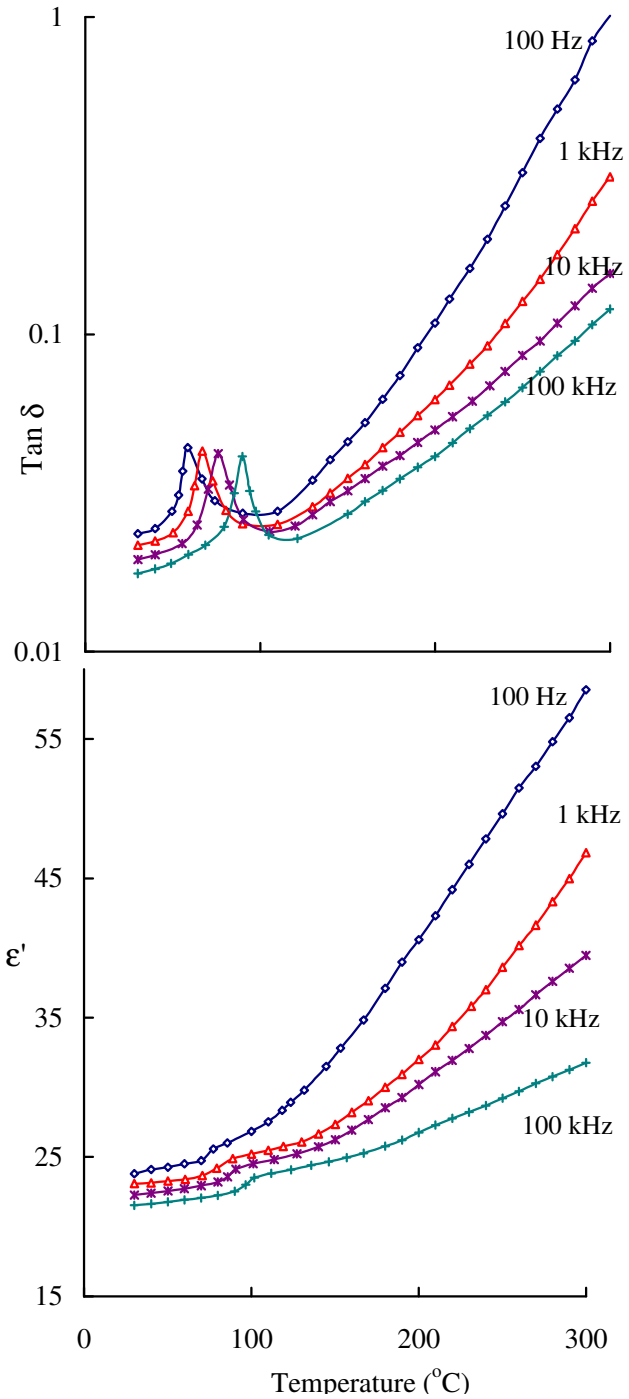

Fig. 4.8 Variation of dielectric constant (ε') and loss (tan δ) with temperature at different frequencies of ZnF_2–As_2O_3–TeO_2 glasses doped with 2.0 mol% of NiO.

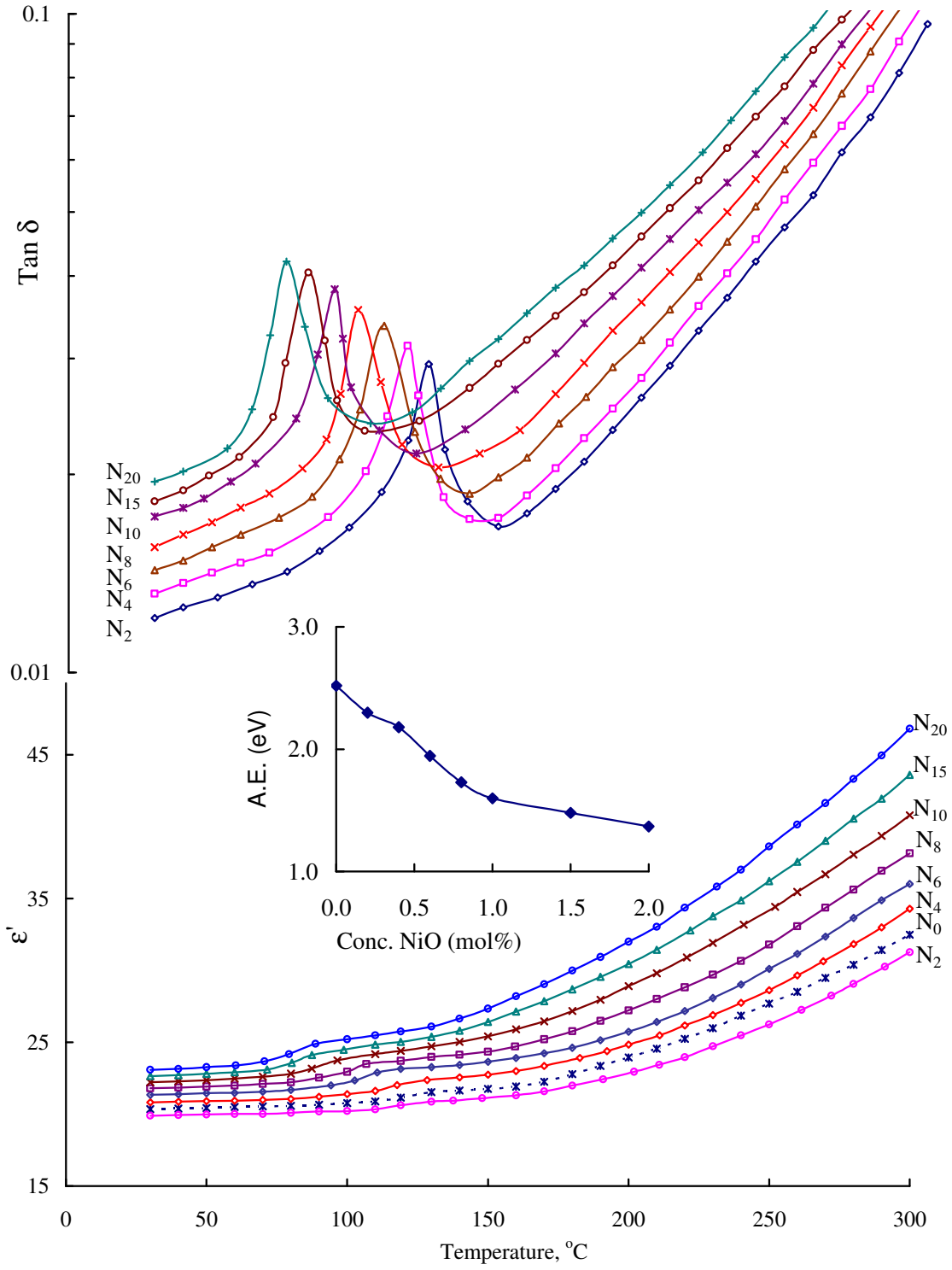

Fig. 4.9 (a) Variation of dielectric constant at 1 kHz (b) variation of loss at 10 kHz with temperature for ZnF_2–As_2O_3–TeO_2:NiO glasses. Inset represents the variation of activation energy for dipoles with the concentration of NiO.

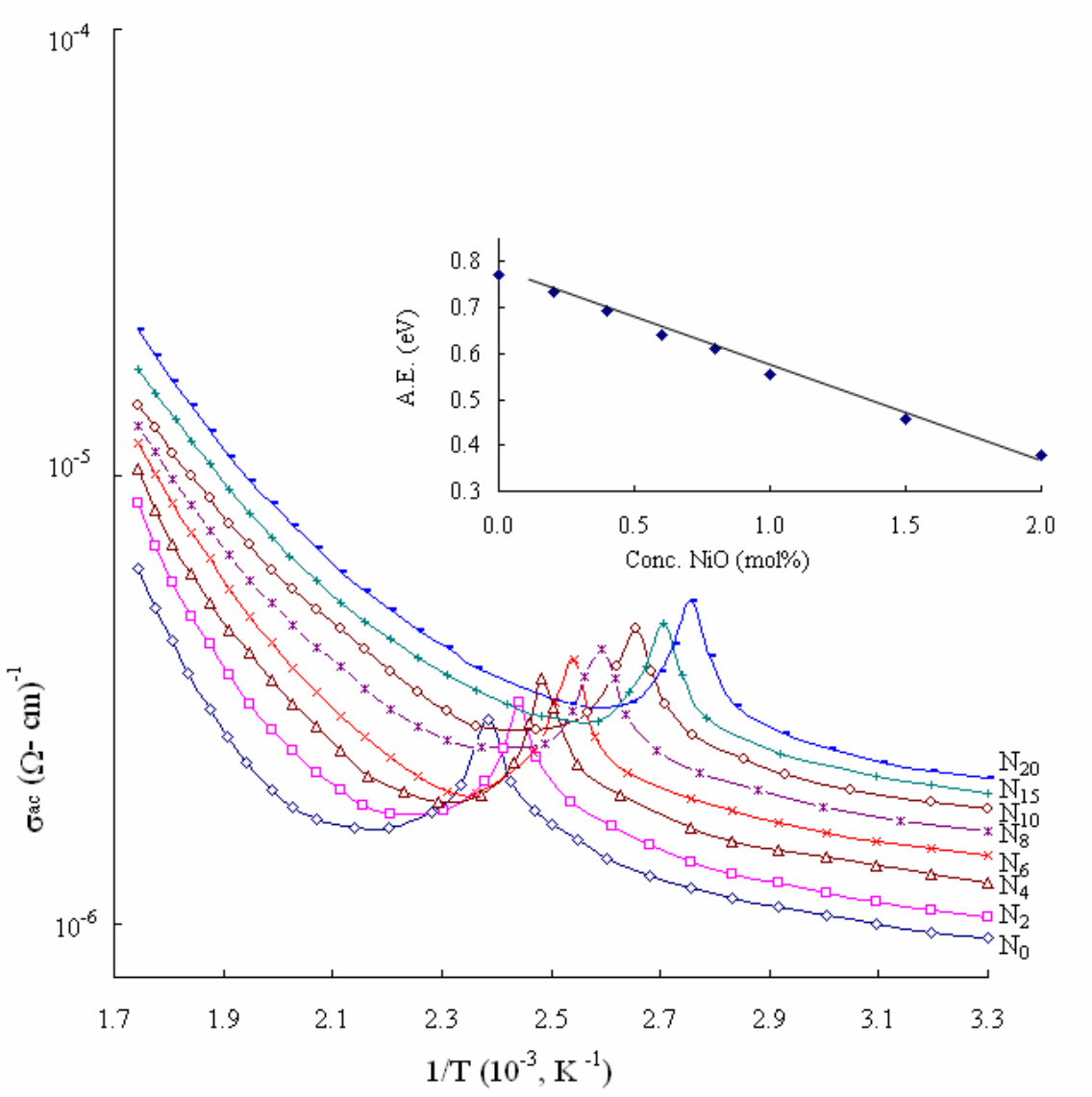

Fig. 4.10 A comparison plot of variation of ac conductivity with 1/T at 100 kHz for ZnF_2–As_2O_3–TeO_2:NiO glasses. Inset shows variation of activation energy with concentration of NiO.

4.4 Discussion

Since the v_2 vibrational frequency range of AsO_3 and TeO_4 structural units is very close to each other as mentioned earlier, there is a possibility for the formation of the linkages of the type Te–O–As in the glass network. The non-resolution of these two vibrational bands in the IR spectra especially for the glasses doped with lower concentration of NiO supports this view point. The oxidation of As^{3+} ions in to As^{5+} also seems to be possible during melting and annealing processes. These As^{5+} ions occupy both tetrahedral and octahedral positions in the glass network; the normal bond length of As^{5+}–O is ~ 1.69 Å [39]. As a participant of glass network, the local structure of As^{5+} cations is more symmetric and the strain energy in the glass network decreases as a whole, thus resulting in a increase in the additional activation energy that is necessary for glass network rearrangement. As a result we expect that less degree of disorder in glasses containing As^{5+} ions rather than in the glasses containing As^{3+} ions. The Ni^{2+} ions seem to exist in both four- and six-fold coordination in the present glass samples. In general, tetragonally positioned Ni^{2+} ions do not induce the formation of any non-bridging oxygen ions, but octahedrally positioned ions may act as modifiers similar to any other transition metal ions that occupy octahedral positions in the glass network [40]. This is also borne out by the fact that the symmetrical vibrational frequencies of ν^{s}_{ax}–TeO_2 bonds of TeO_4 groups in the IR spectra are shifted towards higher

frequencies with decreasing intensity as the concentration of NiO is increased. As modifiers, the Ni^{2+} ions, enter the glass network by breaking up Zn–O–Te, As–O–Te bonds, and TeO_4 bonds and may introduce: (i) the stable Te-O^- and (ii) unstable Te–O^- bonds which will later be modified to Te–O^- (or simply TeO_{3+1}) owing to the contraction of one Te-O^- and the elongation of another Te–O^- bond. With increasing NiO content (up to 0.6 mol%), cleavage of continuous network leads to an increase in the fraction of TeO_{3+1} polyhedra. Further, the elongation of Te–O bond of TeO_{3+1} and its cleavage finally lead to the formation of trigonal prismatic TeO_3 units. Thus in addition to AsO_3, Te–O–Te, Zn–O–Te, As–O–Te linkages, the structure of the present glass network consists of TeO_4, TeO_{3+1} and TeO_3, free Zn^{2+} ions, free F^- ions and non bridging oxygens. Such bonding defects may increase with increase in the concentration of NiO.

The density of ZnF_2–As_2O_3–TeO_2:NiO glasses are observed to depend on the content of NiO. In general, the degree of structural compactness, modification of the geometrical configuration of the glassy network, change in the coordination of the glass-forming ions and fluctuations in the dimensions of the interstitial holes are some of the factors that influence the density of the glass material. Table 4.1 shows a slight increase in density (d) and decrease in molar volume (V_M) with increase in NiO content. The increase in the density is an expected result and can be related to the replacement of TeO_2 (density 5.67

g/cm^3) with NiO (density 6.67 g/cm^3). The molar volume behavior reveals that addition of NiO causes a slight contraction of the glass network.

Recollecting the data on DSC studies, we have observed that the values of the glass transition temperature Tg and glass forming ability parameter K_{gl}, observed to decrease with increase in the concentration of NiO in the glass matrix. Lower values of these parameters indicate lower thermal stability of the glasses. Normally, the decrease in bond length, cross-link density and closeness of packing, are responsible for such a decrease of these parameters. This observation further, points out that there is an increasing concentration of nickel ions that act as modifier with increase in the content of NiO. The presence of arsenic ions in As^{5+} state and also the nickel ions in the tetrahedral positions in large proportions might be responsible for higher values of these parameters for the glasses doped with low concentration of NiO.

Using Tanabe–Sugano diagrams for d^8 ion, the optical absorption spectra of Ni^{2+} doped ZnF_2–As_2O_3–TeO_2 glass were analyzed and the bands O_{h1} and O_{h2} are assigned to the transitions from the $^3A_2$ ground state of octahedrally positioned Ni^{2+} ions to $^3T_2(F)$, and $^3T_1(F)$ excited states respectively. Fig. 4.11 represents TS diagram along with corresponding optical absorption spectrum for the glass N_{10}. In the region of $^3A_2 \rightarrow {}^3T_1(F)$ transition, spin-forbidden transition viz., $^3A_2(F) \rightarrow {}^1E(D)$ due to distorted octahedral site of Ni^{2+} ions may also present [41]. Hence the band observed at about 800 nm may

be considered as superposition of these two transitions. The Racah parameters B and C and the ligand field parameter Dq (crystal field splitting energy) were evaluated using energies of these transitions and the values obtained are given in Table 4.3. The energy level diagram for one of the glass samples (N_{10}) containing various observed transitions, is shown in Fig. 4.12. The kink observed at about 715 nm is attributed to the transition, $^3T_1(F) \rightarrow {}^3T_1(P)$ of Ni^{2+} ions positioned in tetrahedral sites [42]. Thus, the optical absorption spectra of ZnF_2–As_2O_3–TeO_2:NiO glasses indicate that Ni^{2+} ions exist both in octahedral and tetrahedral sites in the network. The tetrahedrally positioned nickel ions participate in the glass network with NiO_4 structural units and alternate with TeO_4 units and strengthen the structure. A schematic illustration of the tellurite arsenate network containing Ni^{2+} in octahedral and tetrahedral positions is shown in Fig. 4.13. Further, the way the intensity of these bands varies with the concentration of NiO suggests that in the glasses that contain smaller concentrations of Ni^{2+} ions, these ions occupy tetrahedral positions and when present in larger concentrations, these ions prefer mostly octahedral sites in the glass network. Using the interelectronic repulsion parameter B, the nephelauxetic ratio was also evaluated using the formula β = B (complex)/B′ (free ion), for all the samples; the value of β is observed to decrease gradually with increase in the concentration of NiO (Table 4.3). This ratio gives information on the delocalization of electrons from the metal ions into

molecular orbitals covering both the metals and ligands. The lower the value of β the greater is the delocalization effect. The lowest value of β obtained for the glass sample N_{20} indicates the maximum delocalization effect in this sample [43].

The variation of the parameter D_q with the concentration of NiO exhibited a decreasing trend (Table 4.3); this dependence is similar to optical band gap. The octahedrally positioned Ni^{2+} ions act as modifiers similar to Zn^{2+} ions and induce non-bridging oxygens in the glass network. The gradual increase in the concentration of octahedral nickel ions in the glass network causes a creation of large number of donor centers. The higher the concentration of these modifier ions, the higher is the concentration of non-bridging oxygens in the glass matrix. This leads to an increase in the degree of localization of electrons thereby increasing the donor centres in the glass matrix. The presence of higher concentrations of these donor centres decreases the optical band gap and shifts the absorption edge towards lower wavelength, as observed (Fig. 4.5).

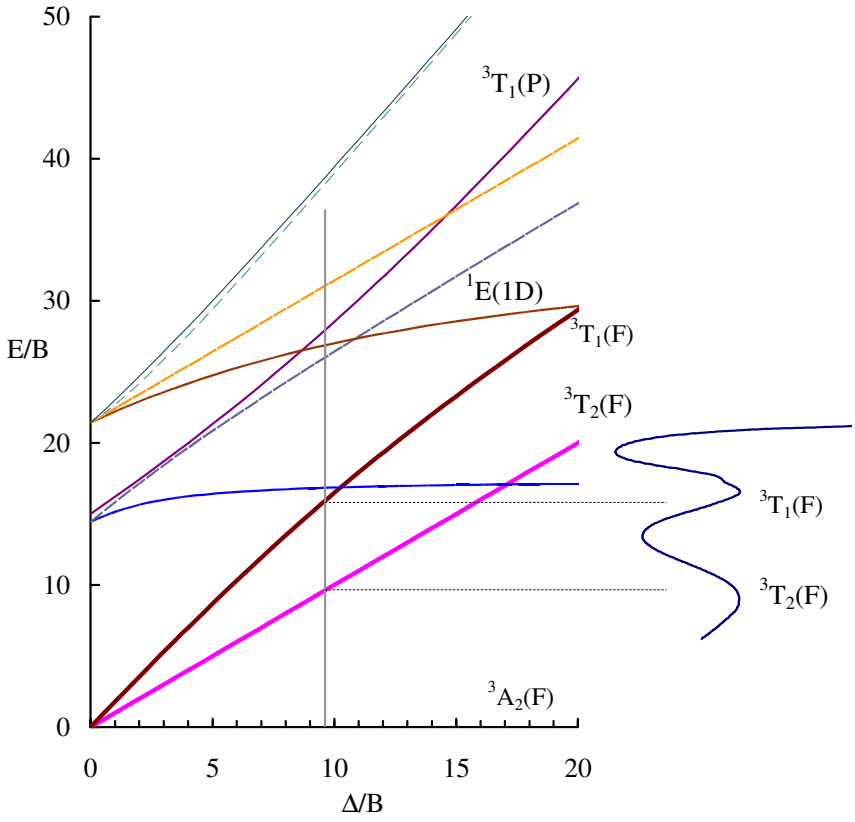

Fig. 4.11 Tanabe–Sugano diagram and corresponding optical absorption spectrum for glass N_{10}.

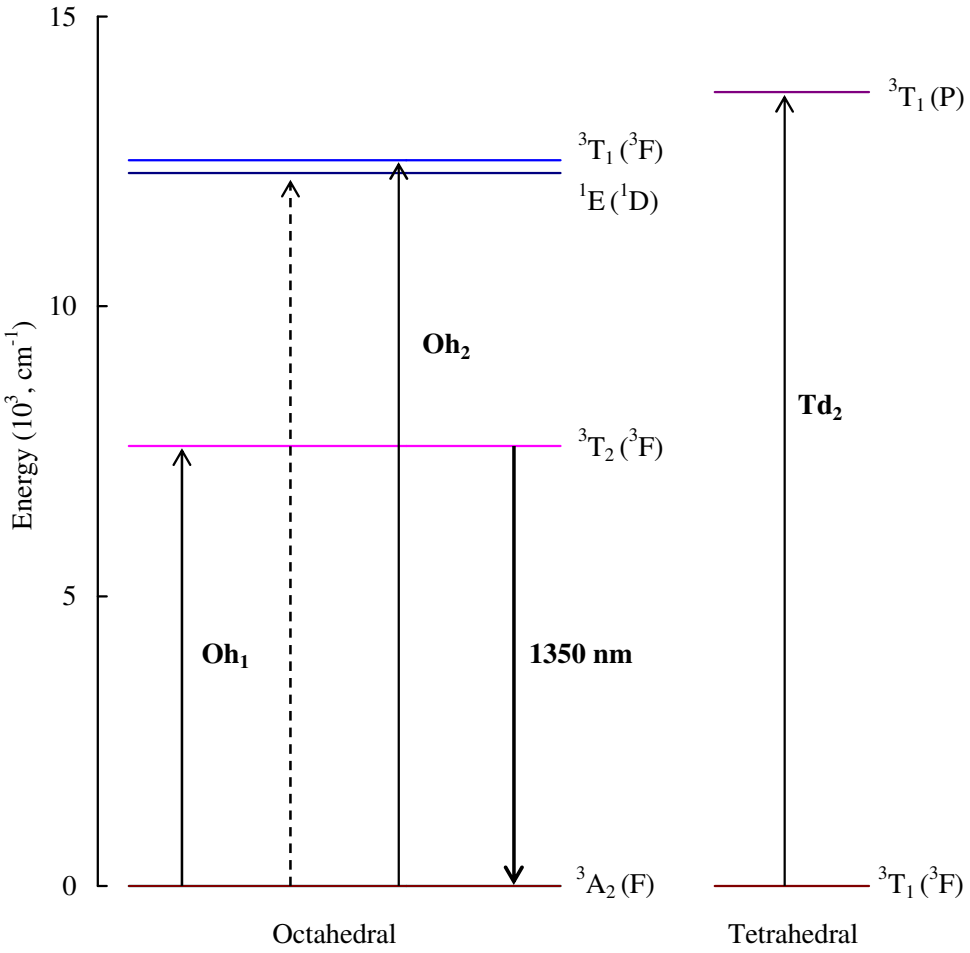

Fig. 4.12 Energy level diagram containing absorption and emission transitions of Ni^{2+} ion in the glass N_{10}.

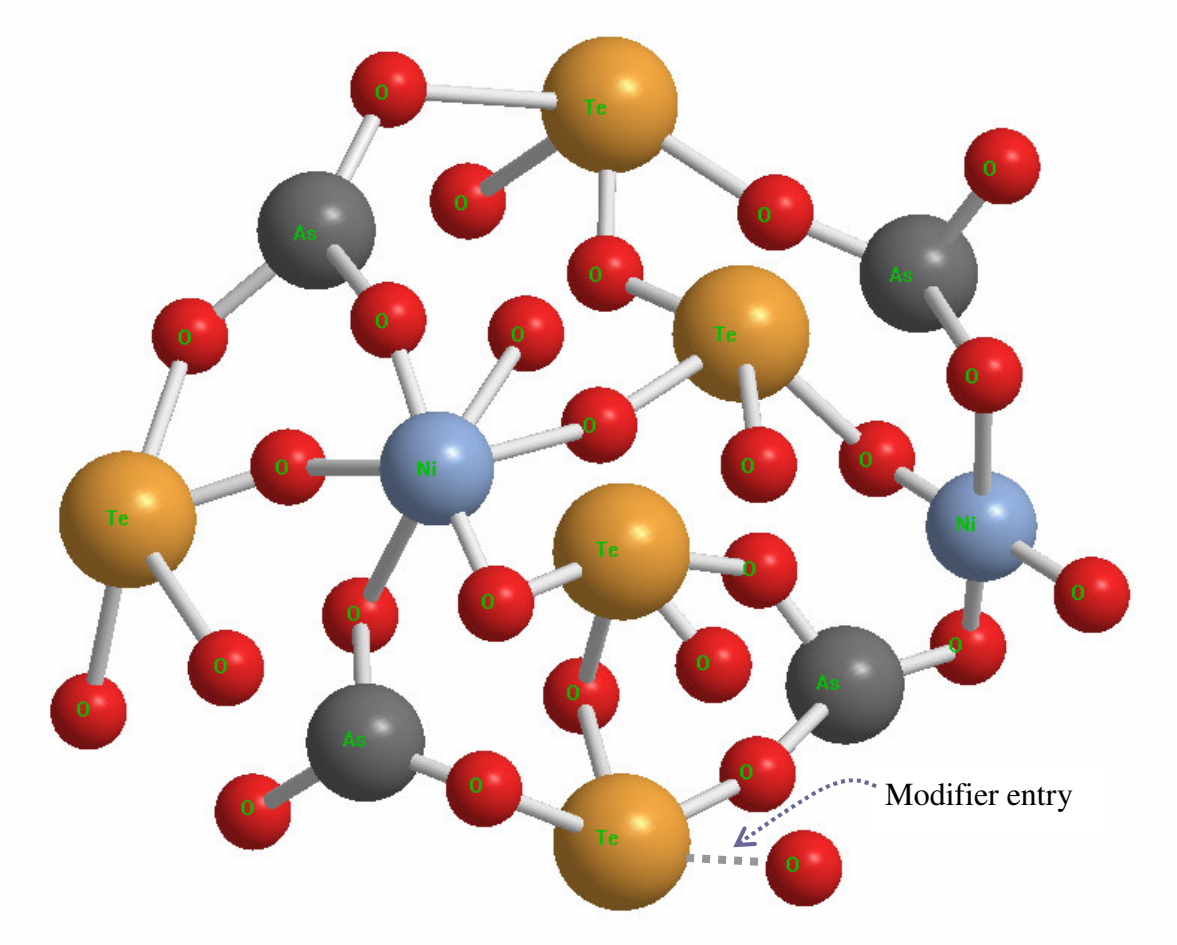

Fig. 4.13 A structural fragmentation of As_2O_3–TeO_2 glass network with the illustration of Ni^{2+} ions in octahedral and tetrahedral positions.

With the gradual increase in the concentration of NiO, the ν_s–TeO_{2ax} and ν_2 of AsO_3 bands in the IR spectra are shifted gradually towards higher frequencies with decreasing intensity. Such changes indicate, decrease in the intensity of symmetrical vibrations of above structural units due to the increasing concentration of modifying ions.

The magnetic properties of ZnF_2–As_2O_3–TeO_2:NiO glass samples arise from the paramagnetic Ni^{2+} (both tetrahedral and octahedral) ions. Magnetically, the octahedral Ni^{2+} complexes have relatively simple behaviour and their magnetic moments are expected to lie in the range 2.9 to 3.4 μ_B [43] depending on the magnitude of the orbital contribution. Since, the ground state $^3T_1$ (F) of tetrahedral Ni^{2+} ions possess much inherent orbital angular momentum, the magnetic moment of perfect tetrahedral Ni^{2+} should be ~ 4.2 μ_B. Even a slight distortion reduces this value markedly because of the orbital degeneracy. The fairly regular tetrahedral complexes of these ions are expected to have the magnetic moment in the range 3.5 to 4.1 μ_B [43]. The gradual decrease of the effective magnetic moment from 3.45 μ_B (for sample N_8) to 3.00 μ_B (for sample N_{20}) confirms that there is a gradual increase of the positions of Ni^{2+} ions in the octahedral sites as the concentration of NiO is increased.

To ascertain further, that there is an increase in the concentration of octahedral sites/modifier positions of Ni^{2+} ions in the glass network, we have

undertaken the dielectric measurements. The dielectric constant of a material is due to electronic, ionic, dipolar and space charge polarizations. Out of these, the space charge contribution depends upon degree of disorder in the glass network. The values of dielectric parameters viz., ε', tan δ and σ_{ac} at any frequency are found to increase with temperature and activation energy for a.c. conduction is observed to decrease with increase in the content of NiO; this is an indication of an increase in the space charge polarization. Such increase indicates the increasing concentration of Ni^{2+} ions that act as modifiers (or that occupy octahedral positions) in these samples. These modifying ions as mentioned earlier, generate bonding defects in the glass network. The defects thus produced create easy path ways for the migration of charges that would build up space charge polarization and facilitate to an increase in the dielectric parameters as observed [44, 45].

We have obtained the increase in the value of $(\tan\delta)_{max}$ and decrease of the effective activation energy associated with the dipoles with increase in the content of NiO in the glass (Table 4.6), these observations suggest an increasing freedom for dipoles to orient in the field direction, obviously due to increasing degree of disorder in glass network. Among the three constituents viz., ZnF_2, As_2O_3 and TeO_2 of these glasses, the bonds of tellurium with oxygen are known to be polar in nature [46] and hence it is reasonable to attribute the observed dipolar effects in these glasses to the TeO_4 structural

units [47, 48]. Further, the way the dielectric loss varies with the temperature for all the samples indicate that there is a spreading of relaxation times. The spreading of dielectric relaxation effects in ZnF_2–As_2O_3–TeO_2 glasses doped with different concentrations of NiO may be attributed to the association of divalent positive ions (Zn^{2+} and also octahedrally positioned Ni^{2+} ions) with a pair of cationic vacancies as observed in a number of conventional glasses, glass ceramics and crystals that contain divalent positive ions as reported before [49, 50]. Thus the data on dielectric loss also point out that there is growing concentration of octahedrally positioned Ni^{2+} ions with increase in the content of NiO in the glass matrix. The increase in the magnitude of ac conductivity and decrease in the activation energy for conduction with the concentration of NiO also supports this view point.

Normally it is the octahedral ion that gives out luminescence emission and so far no emission due to tetrahedral nickel ions has been observed either in glass or crystal hosts. In general, octahedrally coordinated Ni^{2+} ions are expected to give luminescence bands in the green, red and near-infrared regions; out of these the green and red emissions were reported only at very low temperatures [41]. For the present glass system, we have observed (with excitation at 800 nm) a broad band extending from 1200 to 1500 nm with the bary centre shifting towards slightly higher wavelengths with increase in the content of NiO. This emission band is attributed to $^3T_2(3F) \rightarrow {}^3A_2(3F)$

octahedral transition of Ni^{2+} ions. The width and the shape of this transition indicate that there is a relatively increased Stokes shift between the emission and absorption band.

Using the conventional formulae [51], the transition probability,

$$A(\psi_{J'},\psi_J)=\frac{8\nu^2\times10^6}{e^2} \tag{4.2}$$

and the emission cross-section

$$\sigma^E{}_\rho=\frac{\lambda^4 A(\psi_{J'},\psi_J)}{8\pi c n_d{}^2\Delta\lambda} \tag{4.3}$$

of the observed emission peak have been evaluated and presented in Table 4.5 along with the other pertinent data. In Eq. 4.3, n_d is the refractive index of the sample, $\Delta\lambda$ is the half width of the emission peak. The value of $\sigma_p{}^E$ is found to increase gradually from the sample N_2–N_{20} indicating increasing luminescence efficiency with increase in the concentration of the NiO.

4.5 Conclusions

ZnF_2–As_2O_3–TeO_2 glasses doped with different concentrations of NiO have been synthesized. The optical absorption, IR spectra, magnetic susceptibility studies and dielectric properties of these glasses have indicated that there is a growing presence of nickel ions in octahedral positions with increase in the concentration of NiO in the glass matrix. The photoluminescence spectra of these glasses have exhibited a broad emission band due to $^3T_2(3F) \rightarrow {}^3A_2(3F)$ octahedral transition of Ni^{2+} ions in the NIR region. The highest luminescence efficiency is observed for the glass containing 2.0 mol% of NiO. The final analysis further indicated that higher the concentration of octahedrally positioned Ni^{2+} ions, higher is the luminescence efficiency and such glasses may be useful for broad band optical amplifiers in NIR region.

References

[1] G. Murali Krishna, Y. Gandhi, N. Veeraiah, *J. Lumin.* 128 (2008) 631

[2] A.M. Malyarevich, Yu.V. Volk, K.V. Yumashev, V.K. Pavlovskii, S.S. zapalov, O.S. Dymshits, A.A. Zhilin, *J. Non-Cryst. Solids* 351 (2005) 3551.

[3] M. Srinivasa Reddy, S.V.G.V.A. Prasad, N. Veeraiah, *Phys. Stat. Sol. (a),* 204 (2007) 816.

[4] B.V. Raghavaiah, C. Laxmikanth, N. Veeraiah, *Optics Commun.* 235 (2004) 341.

[5] N. Krishna Mohan, M. Rami Reddy, N. Veeraiah, *J. Alloys Compd.* 458 (2008) 66.

[6] H. Keppler, N. Bagdassarov, *Chem. Geo.* 158 (1999) 105.

[7] E. Zannoni, E. Cavalli, M. Bettinelli, *J. Phys. Chem. Solids* 67 (2006) 789.

[8] G. Feng, S. Zhou, J. Bao, S. Xu, J. Qiu, *J. Alloys Compd.* 457 (2008) 506.

[9] D. Souri, S.A. Salehizadeh, *J. Mater. Sci.* 44 (2009) 5800.

[10] F.A. Moustaffa, F.H. El-Batal, A.M. Fayadd, I.M. El-Kashef, *Acta Phys. Polo. A* 117 (2010) 471.

[11] R. Kumar, A. Arvind, M. Goswami, S. Bhattacharya, V.K. Shrikhande, G.P. Kothiyal, *J. Mater. Sci.* 44 (2009) 3349.

[12] P.S. Prasad, V.R. Kumar, G.N. Raju, N. Veeraiah, *Mater. Sci.-Poland* 26 (2008) 527.

[13] J. Bao, S. Zhou, G. Feng, X. Wang, X. Qiao, J. Qiu, *J. Alloys Compd.* 456 (2008) 239.

[14] M. Kusatsugu, M. Kanno, T. Honma, T. Komatsu, *J. Solid State Chem.* 181 (2008) 1176

[15] S. Wang, K. Liang, *J. Non-Cryst. Solids* 354 (2008) 1522.

[16] M. Sato, T. Honma, Y. Benino, T. Komatsu, *J. Solid State Chem.* 180 (2007) 2541

[17] B. Wu, J. Qiu, M. Peng, J. Ren, X. Jiang, C. Zhu, *Mater. Res. Bull.* 42 (2007) 762.

[18] E. Mejia-Ramirez, A. Gorokhovsky, J.I. Escalante-Garcia, *J. Non-Cryst. Solids* 353 (2007) 366.

[19] T. Suzuki, Y. Arai, Y. Ohishi, *J. Non-Cryst. Solids* 353 (2007) 36.

[20] T. Suzuki, Y. Nakatsubata, G.S. Murugan, Y. Ohishi, *Ceram. Trans.* 197 (2006) 13

[21] B. Brendeback, R. Glaum, M. Funke, F. Reinauer, J. Hormes and H. Modrow, *Z. Naturforsch* 60a (2005) 449.

[22] H. Schlenz, F. Reinauer, R. Glaum, J. Neuefeind, B. Brendebach and J. Hormes, *J. Non-Cryst. Solids* 351 (2005) 1014.

[23] P. Nageswara Rao, G. Naga Raju, D. Krishna Rao, N. Veeraiah, *J. Lumin*. 117 (2006) 53.

[24] M. Tawati Daefalla, M.J.B. Adlan, *Ceram. Int.* 30 (2004) 1737.

[25] T.K. Kundu, D.K. Chakravorty, *J. Mater. Res.* 14 (1999) 1069.

[26] R.S. Singh, S.P. Singh, *Phys. Chem. Glasses* 40 (1999) 235.

[27] El-Desoky, S.M. Mohamed, I. Kashif, *J. Mater. Sci. Mater. Electr.* 10 (1999) 279.

[28] V. Rajendran, F.A Khalifa, H.A. El-Batal, Ind. *J. Pure. Appl. Phys.* 35 (1997) 618.

[29] M. Shibata, M. Ookawa, T. Yokokawa, *J. Non-Cryst. Solids* 190 (1995) 226.

[30] A. Musinu, G. Piccaluga, P.H. Gaskell, *J. Non-Cryst. Solids* 192 (1995) 32.

[31] A. Corrias, A. Musinu and P.H. Gaskell, *J. Non-Cryst. Solids* 192 (1995) 49.

[32] I. Kashif, H. Farouk, S.A. Aly, *J. Mater. Sci. Mater. Electr.* 2 (1991) 216.

[33] F.A. Khalifa, Z.A. El-hadi, F.M. Ezz, *J. Mater. Sci. Lett.* 10 (1991) 1184.

[34] J.L. Rao, G.L. Narendra and S.V.J. Lakshman, *Polyhedron* 9 (1990)1475.

[35] E. Baiocchi, M. Bettinelli, *J. Non-Cryst. Solids* 46 (1981) 203.

[36] A. Paul and A.N. Tiwari, *J. Mater. Sci.* 9 (1974) 1057.

[37] I. Morozova, A. Yakind, *Fis. Khim. Stekla* 3 (1977) 197.

[38] O. Miroschnichenko, O. Klimaschevski, *Neorg. Mater.* 6 (1970) 1893.

[39] J.M. Charnock, D.A. Polya, A.G. Gault and R.A. Wogelius, *Am. Mineralogist* 921 (2007) 856.

[40] G. Murali Krishna, B. Anila Kumari, M. Srinivasa Reddy and N. Veeraiah, *J. Solid State Chem.* 180 (2007) 2747.

[41] E. Zannoni, E. Cavalli, A. Toncelli, M. Tonelli, M. Bettinelli, *J. Phys. Chem. Sol.* 60 (1999) 449.

[42] J.L. Rao, G. L. Narendra, and S.V.J. Laksmana, *Polyhedron* 9 (1990) 1475.

[43] J.D. Lee, *Concise Inorganic Chemistry*, 5th ed. (Blackwell Science, 1996).

[44] L. Srinivasa Rao, M. Srinivasa Reddy, D. Krishna Rao, N. Veeraiah, *J. Solid State Sci.* 11 (2009) 578.

[45] T. Satyanarayana, I.V. Kityk, M. Piasecki, P. Bragiel, M.G. Brik, Y. Gandhi and N. Veeraiah, *J. Phys.–Cond. Matter* 21 (2009) 245104

[46] V.R. Kumar, N. Veeraiah and S. Buddudu, *J. de Phys. III,* 7 (1997) 951.

[47] A. Singh, V. K. Dhawan, *Phil. Mag. B* 48 (1983) 215.

[48] D.K. Durga, N. Veeraiah, *J. Mater. Sci.* 36 (2001) 5625.

[49] S.V.G.V.A. Prasad, M. Srinivasa Reddy, N. Veeraiah, *J. Phys. Chem. Solids* 67 (2006) 2478.

[50] G. Murali Krishna, Y. Gandhi and N. Veeraiah*, Physica Status Solidi(a)* 205 (2008) 177.

[51] G. Fuxi, *Optical and Spectroscopic Properties of Glass*, Springer-Verlag, Shanghai Scientific Technical Pub., Shanghai, 1991.